Symbolic-Numerical Calculations of High-$|m|$ Rydberg States and Decay Rates in Strong Magnetic Fields*

Alexander Gusev, Sergue Vinitsky, Ochbadrakh Chuluunbaatar, Vladimir Gerdt, Luong Le Hai, and Vitaly Rostovtsev **

Joint Institute for Nuclear Research, Dubna, Moscow Region, Russia
gooseff@jinr.ru, vinitsky@theor.jinr.ru

Abstract. Symbolic-numeric solving of the boundary value problem for the Schrödinger equation in cylindrical coordinates is given. This problem describes the impurity states of a quantum wire or a hydrogen-like atom in a strong homogeneous magnetic field. It is solved by applying the Kantorovich method that reduces the problem to the boundary-value problem for a set of ordinary differential equations with respect to the longitudinal variables. The effective potentials of these equations are given by integrals over the transverse variable. The integrands are products of the transverse basis functions depending on the longitudinal variable as a parameter and their first derivatives. To solve the problem at high magnetic quantum numbers $|m|$ and study its solutions we present an algorithm implemented in Maple that allows to obtain *analytic expressions* for the effective potentials and for the transverse dipole moment matrix elements. The efficiency and accuracy of the derived algorithm and that of Kantorovich numerical scheme are confirmed by calculating eigenenergies and eigenfunctions, dipole moments and decay rates of low-excited Rydberg states at high $|m| \sim 200$ of a hydrogen atom in the laboratory homogeneous magnetic field $\gamma \sim 2.35 \times 10^{-5} (B \sim 6T)$.

1 Introduction

In earlier papers, we considered the application of the Kantorovich method for solving the discrete- and continuous-spectrum boundary-value problems (BVP) [1] for hydrogen-like atoms in magnetic field and the ion axial channelling problem in a crystal. The approach implies the use of a parametric basis of oblate spheroidal angular functions in spherical coordinates where the radial variable runs a semi-axis [2,3,4,5]. The method has been further developed in connection with calculations of spectral and optical characteristics of model semiconductor nanostructures, namely, quantum dots(QD), quantum wells(QW) and quantum

* This work was partially supported by the RFBR Grants Nos. 10-02-00200 and 11-01-00523.

** The coauthors (AG, SV, OC, VG, and LH) congratulate Vitaly Rostovtsev on turning 20 for the fourth time.

V.P. Gerdt et al. (Eds.): CASC 2012, LNCS 7442, pp. 155–171, 2012.

wires(QWr) [6,7,8,9]. For this purpose we used different parametric basis functions in appropriate coordinate systems. The functions were calculated by solving parametric eigenvalue problems by means of the program ODPEVP [10].

Taking into account the growing interest in problems possessing axial symmetry, like impurity states of QWr's or high-angular-momentum Rydberg states and quasi-stationary states imbedded in continuum of a hydrogen atom in magneto-optical traps [11,12,13], it is imperative to implement the Kantorovich scheme for solving the BVP for the longitudinal variable running the whole axis of a cylindrical coordinate system[8,9]. This would allow direct calculation of the main characteristics of a multichannel scattering problem, such as reflection and transmission coefficients matrices, recombination rates and ionization cross-sections for Rydberg states, and decay rates of the lowest bound states of manifolds with high values of the magnetic quantum number $|m|$ [11,12,13].

For the Schrödinger equation describing a hydrogen-like atom in a strong homogeneous magnetic field, the boundary-value problem (BVP) in cylindrical coordinates is reduced to solving a set of the longitudinal equations in the framework of the Kantorovich method. The effective potentials of these equations are given by integrals over the transverse variable, the integrands being products of transverse basis functions, depending on the longitudinal variable as a parameter, and their first derivatives with respect to the parameter. One can say that at high $|m|$, the discrete-spectrum problem is described by a system of two coupled 2D- and 1D-oscillators corresponding to the transverse ρ and longitudinal z variables, with the frequencies ω_ρ and ω_z, respectively. To analyze the low-excited Rydberg states of such system it is useful to have the solution *in an analytic form*. Indeed, for high $|m|$ we can consider the Coulomb potential as a perturbation with respect to the transversal centrifugal potential and the oscillator potential with the frequency $\omega_\rho = \gamma/2$. For the laboratory magnetic field $B = B_0\gamma \sim 6T$, i.e., $\gamma \sim 2.35 \times 10^{-5}$, this is true at the *adiabatic parameter* values $\tilde{m} \sim 5.89$, where $\tilde{m}$ is defined as $\tilde{m} = (\omega_\rho/\omega_z)^{4/3} = |m|\gamma^{1/3}$. Under the condition $|m| \geq 6\gamma^{-1/3}$ we can approximate the Coulomb potential by a Taylor expansion in powers of the auxiliary transverse variable with respect to a specially chosen point with given accuracy in the region of its convergence. Then we can find the approximate transversal eigenvalues and eigenfunctions depending parametrically on the longitudinal variable, in the framework of a perturbation scheme and by using the eigenvalues and eigenfunctions of the 2D oscillator as unperturbed ones. To express *analytically* the transverse basis functions and eigenvalues, the corresponding effective potentials, and the transverse dipole moment matrix elements as well as perturbation solution of the BVP, we elaborate a symbolic-numerical algorithm (SNA) implemented in Maple. The efficiency and accuracy of the algorithm and that of the derived Kantorovich numerical scheme are confirmed by computation of eigenenergies and eigenfunctions, dipole moments and decay rates for the manifolds of high-$|m|$ low-excited Rydberg states of a hydrogen atom in the laboratory homogeneous magnetic field, and by comparison with the results obtained by other methods.

The paper is organized as follows. In Section 2, we briefly describe the reduction by the KM of the 3D eigenvalue problem at fixed values $|m|$ of magnetic quantum number to the 1D eigenvalue problem for a set of close-coupled longitudinal equations. In Sections 3 and 4, the algorithm for calculating the effective potentials and the transverse dipole moment matrix elements *in the analytic form* at large values of $|m|$ is presented. The algorithm has been implemented in Maple. To find the validity range of the method, in Section 5 we compare our results with the known ones obtained in the cylindrical coordinates. Decay rates of the lowest bound states of manifolds with high magnetic quantum number $|m|$ are also presented here. In Section 6, we conclude and discuss possible future applications of the described method.

2 Problem Statement in Cylindrical Coordinates

The component $\Psi(\rho, z)$ of the wave function $\Psi(\rho, z, \varphi) = \Psi(\rho, z) \exp(\imath m\varphi)/\sqrt{2\pi}$ of a hydrogen atom in an axially symmetric magnetic field $\boldsymbol{B} = (0, 0, B)$ in the cylindrical coordinates (ρ, z, φ) satisfies the 2D Schrödinger equation in the region $\Omega_c = \{0 < \rho < \infty \text{ and } -\infty < z < \infty\}$:

$$-\frac{\partial^2}{\partial z^2}\Psi(\rho, z) + A_c\Psi(\rho, z) = \epsilon\Psi(\rho, z), \quad A_c = -\frac{1}{\rho}\frac{\partial}{\partial\rho}\rho\frac{\partial}{\partial\rho} + m\gamma + U(\rho, z), \tag{1}$$

$$U(\rho, z) = \frac{m^2}{\rho^2} + \frac{\gamma^2\rho^2}{4} + V_c(\rho, z), \quad V_c(\rho, z) = -\frac{2q}{\sqrt{\rho^2 + z^2}}. \tag{2}$$

Here $m = 0, \pm1, \ldots$ is the magnetic quantum number, $\gamma = B/B_0 = \hbar\omega_c/(2Ry)$, $B_0 \cong 2.35 \times 10^5\, T$ is a dimensionless parameter which determines the field strength B, $\omega_c = eB/(m_e c) = eB_0\gamma/(m_e c)$ is the cyclotron frequency, and $U(\rho, z)$ is the potential energy (see Fig. 1a), q is Coulomb charge of nucleus. We use the atomic units $(a.u.)$ $\hbar = m_e = e = 1$ and assume the mass of the nucleus to be infinite. In these expressions, $\epsilon = 2E$, E is the energy (expressed in Rydbergs, $1\, Ry = (1/2)\, a.u.$) of the bound state $|m\sigma\rangle$ with fixed values of m and z-parity $\sigma = \pm1$, and $\Psi(\rho, z) \equiv \Psi^{m\sigma}(\rho, z) = \sigma\Psi^{m\sigma}(\rho, -z)$ is the corresponding wave function. The boundary conditions in each $m\sigma$ subspace $L_2(\Omega)$ of the complete Hilbert space have the form

$$\lim_{\rho\to0} \rho\frac{\partial\Psi(\rho, z)}{\partial\rho} = 0, \quad \text{for} \quad m = 0, \quad \text{and} \quad \Psi(0, z) = 0, \quad \text{for} \quad m \neq 0, \tag{3}$$

$$\lim_{\rho\to\infty} \Psi(\rho, z) = 0. \tag{4}$$

The eigenfunction $\Psi(\rho, z) \equiv \Psi_t(\rho, z) \in L_2(\Omega)$ of the discrete real-valued spectrum $\epsilon : \epsilon_1 < \epsilon_2 < \cdots \epsilon_t < \cdots < \gamma$ obeys the asymptotic boundary condition. Approximately this condition is replaced by the boundary condition of the second and/or first type at small and large $|z|$, but finite $|z| = z_{\max} \gg 1$,

$$\lim_{z\to0} \frac{\partial\Psi(\rho, z)}{\partial z} = 0, \quad \sigma = +1, \quad \Psi(\rho, 0) = 0, \quad \sigma = -1, \tag{5}$$

$$\lim_{z\to\pm\infty} \Psi(\rho, z) = 0 \quad \to \quad \Psi(\rho, \pm|z_{\max}|) = 0. \tag{6}$$

In numerical calculation of the eigenvalues and eigenfunctions with given accuracy by programs KANTBP2 and ODPEVP realizing the finite element method, we used computational schemes derived from the Rayleigh–Ritz variational functional [1,10]

$$\mathcal{R}(\Psi_t,\epsilon_t)=\Bigg(\int\limits_{-z_{\max}}^{z_{\max}}dz\int\limits_{0}^{\infty}\rho d\rho\frac{\partial\Psi_t(\rho,z)}{\partial z}\frac{\partial\Psi_t(\rho,z)}{\partial z}+\frac{\partial\Psi_t(\rho,z)}{\partial\rho}\frac{\partial\Psi_t(\rho,z)}{\partial\rho} \tag{7}$$

$$+\Psi_t(\rho,z)(m\gamma+U(\rho,z))\Psi_t(\rho,z)\Bigg)\Big/\int_{-z_{\max}}^{z_{\max}}dz\int_0^{\infty}\rho d\rho\Psi_t(\rho,z)\Psi_{t'}(\rho,z)$$

with the additional normalization and orthogonality conditions

$$\langle t|t'\rangle=\int_{-z_{\max}}^{z_{\max}}dz\int_0^{\infty}\rho d\rho\Psi_t(\rho,z)\Psi_{t'}(\rho,z)=2\int_0^{z_{\max}}dz\int_0^{\infty}\rho d\rho\Psi_t(\rho,z)\Psi_{t'}(\rho,z)=\delta_{tt'}. \tag{8}$$

For $m\neq 0$ eigenfunctions $\Psi_t(\rho,z)\sim\rho^{|m|/2}$ at small ρ. So, in numerical calculations, a reduced interval $[0<\rho_{\min},\rho_{\max}\gg 1]$ is conventionally used [8].

2.1 Kantorovich Reduction

Consider a formal expansion of the partial solution $\Psi_t^{m\sigma}(\rho,z)$ of Eqs. (1)–(4) corresponding to the eigenstate $|m\sigma t\rangle$ expanded in the finite set of one-dimensional basis functions $\{B_j^m(\rho;z)\}_{j=1}^{j_{\max}}$

$$\Psi_t^{m\sigma}(\rho,z)=\sum_{j=1}^{j_{\max}}B_j^m(\rho;z)\chi_j^{(m\sigma t)}(z). \tag{9}$$

In Eq. (9), the functions $\boldsymbol{\chi}^{(t)}(z)\equiv\boldsymbol{\chi}^{(m\sigma t)}(z)$, $(\boldsymbol{\chi}^{(t)}(z))^T=(\chi_1^{(t)}(z),\ldots,\chi_{j_{\max}}^{(t)}(z))$ are unknown, and the surface functions $\boldsymbol{B}(\rho;z)=\boldsymbol{B}^m(\rho;-z)$, $(\boldsymbol{B}(\rho;z))^T=(B_1(\rho;z),\ldots,B_{j_{\max}}(\rho;z))$ form an orthonormal basis for each value of the variable $z\in\mathcal{R}$ which is treated as a parameter.

In KM, the wave functions $B_j(\rho;z)$ (see Fig. 2) and the potential curves $E_j(z)$ (in Ry) are determined as solutions of the following eigenvalue problem

$$A_cB_j(\rho;z)=E_j(z)B_j(\rho;z), \tag{10}$$

with the operator A_c from (1)–(2) and the boundary conditions (3), (4) at each fixed $z\in\mathcal{R}$. Since the operator in the left-hand side of Eq. (10) is self-adjoint, its eigenfunctions are orthonormal

$$\left\langle B_i(\rho;z)\middle|B_j(\rho;z)\right\rangle_{\rho}=\int_0^{\infty}B_i(\rho;z)B_j(\rho;z)\rho d\rho=\delta_{ij}, \tag{11}$$

where δ_{ij} is the Kronecker symbol. Therefore, we transform the solution of the above problem into the solution of an eigenvalue problem for a set of $j_{\max}$

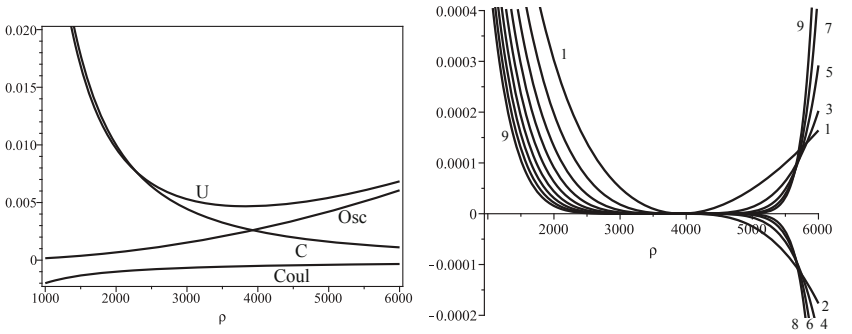

Fig. 1. Left panel: the profile of potential energy $U(\rho,z)=m^2/\rho^2+\gamma^2\rho^2/4+V_c(\rho,z)$ (U) in the plane $z=0$ and its components, namely, the centrifugal (C), oscillator (Osc), and Coulomb (Coul) potentials. Right panel: the approximation errors $\delta U^{(j_{\max})}(\rho,z)\equiv\sum_{i=1}^{j_{\max}}U^{(i)}(\rho,z)-U(\rho,z)$ $(j_{\max}=1,...,9)$ of the potential energy $U(\rho,z=0)$. Here $q=-1$, $m=-200$, $\gamma=2.553191\cdot10^{-5}$ ($B=6$T, $\tilde{m}\approx5.89$)

ordinary second-order differential equations that determines the energy ϵ and the coefficients $\boldsymbol{\chi}^{(i)}(z)$ of the expansion (9)

$$\left(-\mathbf{I}\frac{d^2}{dz^2}+\mathbf{U}(z)+\mathbf{Q}(z)\frac{d}{dz}+\frac{d\mathbf{Q}(z)}{dz}\right)\boldsymbol{\chi}^{(t)}(z)=\epsilon_t\mathbf{I}\boldsymbol{\chi}^{(t)}(z). \tag{12}$$

Here $\mathbf{I}$, $\mathbf{U}(z)=\mathbf{U}(-z)$, and $\mathbf{Q}(z)=-\mathbf{Q}(-z)$ are the $j_{\max}\times j_{\max}$ matrices whose elements are expressed as

$$U_{ij}(z)=E_i(z)\delta_{ij}+H_{ij}(z),\quad H_{ij}(z)=\int_0^\infty\frac{\partial B_i(\rho;z)}{\partial z}\frac{\partial B_j(\rho;z)}{\partial z}\rho d\rho, \tag{13}$$

$$I_{ij}(z)=\delta_{ij},\quad Q_{ij}(z)=-Q_{ji}(z)=-\int_0^\infty B_i(\rho;z)\frac{\partial B_j(\rho;z)}{\partial z}\rho d\rho.$$

The discrete spectrum solutions $\epsilon:\epsilon_1<\epsilon_2<\cdots\epsilon_t<\cdots<\gamma$ at fixed m and parity $\sigma=\pm1$ obey the asymptotic boundary condition and are orthonormal

$$\lim_{z\to0}\left(\frac{d}{dz}-\mathbf{Q}(z)\right)\boldsymbol{\chi}^{(t)}(z)=0,\quad\sigma=+1,\quad\boldsymbol{\chi}^{(t)}(0)=0,\quad\sigma=-1, \tag{14}$$

$$\lim_{z\to\pm\infty}\boldsymbol{\chi}^{(t)}(z)=0\quad\to\quad\boldsymbol{\chi}^{(t)}(\pm z_{\max})=0, \tag{15}$$

$$\int_{-z_{\max}}^{z_{\max}}\left(\boldsymbol{\chi}^{(t)}(z)\right)^T\boldsymbol{\chi}^{(t')}(z)dz=2\int_0^{z_{\max}}\left(\boldsymbol{\chi}^{(t)}(z)\right)^T\boldsymbol{\chi}^{(t')}(z)dz=\delta_{tt'}. \tag{16}$$

Remark 1. In diagonal adiabatic approximation

$$\left(-\frac{d^2}{dz^2}+U_{jj}(z)\right)\chi_j^{(v)}(z)=\epsilon_{jv}\chi_j^{(v)}(z) \tag{17}$$

discrete spectrum $\epsilon:\epsilon_{j1}<\epsilon_{j2}<\cdots\epsilon_{jv}<\cdots<\gamma$ numerated by number v that determines the number $v-1$ of nodes of the solution $\chi_j^{(v)}(z)$ at fixed value j.

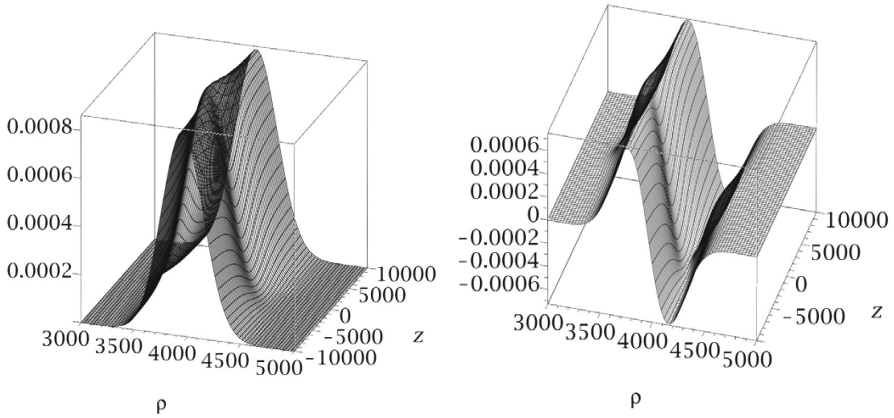

Fig. 2. The basis functions B_1 and B_2 for $m = -200$, $q = 1$, $\gamma = 2.553191 \cdot 10^{-5}$

3 Solving the Parametric Eigenvalue Problem at Large $|m|$

Step 1. In (10), (11) apply the transformation to a scaled variable x

$$x = \frac{\gamma\rho^2}{2}, \quad \rho = \frac{\sqrt{x}}{\sqrt{\gamma/2}}, \tag{18}$$

and put $\lambda_j(z) = E_j(z)/(2\gamma) = \lambda_j^{(0)} + m/2 + \delta\lambda_j(z)$, where $\lambda_j^{(0)} = n + (|m|+1)/2$. The eigenvalue problem reads

$$\left(-\frac{\partial}{\partial x} x \frac{\partial}{\partial x} + \frac{m^2}{4x} + \frac{x}{4} + \frac{m}{2} - \frac{q}{\gamma\sqrt{\frac{2x}{\gamma} + z^2}} - \lambda_j \right) B_j(x; z) = 0, \tag{19}$$

with a normalization condition

$$\frac{1}{\gamma} \int_0^\infty B_j(x; z)^2 dx = 1. \tag{20}$$

At $q = 0$, Eq. (19) without $m/2$ takes the form

$$L(n) B_j^{(0)}(x) = 0, \qquad L(n) = -\frac{\partial}{\partial x} x \frac{\partial}{\partial x} + \frac{m^2}{4x} + \frac{x}{4} - \lambda_j^{(0)}, \tag{21}$$

and has the regular and bounded solutions at

$$\lambda_j^{(0)} = n + (|m| + 1)/2, \tag{22}$$

where the transverse quantum number $n \equiv N_\rho = j - 1 = 0, 1, \ldots$ determines the number of nodes of the solution $B_j^{(0)}(x) \equiv B_{nm}^{(0)}(x)$ with respect to the variable x. The normalized solutions of Eq. (21) take the form

$$B_j^{(0)}(x) = C_{n|m|} e^{-\frac{x}{2}} x^{\frac{|m|}{2}} L_n^{|m|}(x), \qquad C_{n|m|} = \left[\gamma \frac{n!}{(n+|m|)!}\right]^{\frac{1}{2}}, \tag{23}$$

$$\frac{1}{\gamma}\int_0^\infty B_{nm}^{(0)}(x) B_{n'm}^{(0)}(x) dx = \delta_{nn'}, \tag{24}$$

where $L_n^{|m|}(x)$ are Laguerre polynomials [14].

Step 2. Substituting the notation $\delta\lambda_j(z) = \lambda_j(z) - \lambda_j^{(0)} - m/2 \equiv E_j(z)/(2\gamma) - (n + (m + |m| + 1)/2)$, and the Taylor expansion in the vicinity of the point $x_0 = x_s\gamma$:

$$V_c(x,z) = -\frac{q}{\gamma\sqrt{\frac{2x}{\gamma}+z^2}} = -\sum_{k=1}^{j_{\max}} V^{(k)}(x,z)\varepsilon^k = -\frac{\varepsilon q}{\gamma(z^2+2x_s)^{1/2}} \tag{25}$$

$$+\frac{\varepsilon q(x-x_s\gamma)}{\gamma^2(z^2+2x_s)^{3/2}} - \frac{3\varepsilon^2 q(x-x_s\gamma)^2}{2\gamma^3(z^2+2x_s)^{5/2}} + \frac{5\varepsilon^3 q(x-x_s\gamma)^3}{2\gamma^4(z^2+2x_s)^{7/2}} + O\left(\frac{\varepsilon^4}{(z^2+2x_s)^{9/2}}\right),$$

into Eq. (19) at $q \neq 0$, transform it to the following form

$$L(n)B_j(x;z) + \left(\sum_{k=1}^{j_{\max}} V^{(k)}(z)\varepsilon^k - \delta\lambda_j(z)\right) B_j(x;z) = 0. \tag{26}$$

Here ε is a formal parameter that will be put to be 1 in the final expression. The parameters $x_s = \rho_s^2/2$ and ρ_s approximately correspond to the minimum of the potential energy (2). In so doing, the Coulomb term is neglected. In the calculations we choose $\rho_s = \sqrt{2|m|/\gamma}$ under assumption that the condition $\gamma^2\rho^2/4 + m^2/\rho^2 \gg 2|q|/\rho$ is valid. The approximation errors $\delta U^{(j_{\max})}(\rho, z)$ at $j_{\max} = 1, ..., 9$ are illustrated in Fig. 1b. One can see that in the localization interval $\rho \in [3000, 5000]$ of the eigenfunction (19), the errors decrease with increasing order $j_{\max}$ (see Fig. 2). Performing Taylor expansion at $|z|/\rho_s \gg 1$, we arrive at the inverse power series that gives the same results as the perturbation theory in powers of $1/|z|$ [8].

Step 3. The solution of Eq. (26) is found in the form of perturbation expansion in powers of ε

$$\delta\lambda_j(z) = \sum_{k=1}^{k_{\max}} \varepsilon^k \lambda_n^{(k)}(z), \quad B_j(x;z) = B_n^{(0)}(x) + \sum_{k=0}^{k_{\max}} \varepsilon^k B_n^{(k)}(x,z). \tag{27}$$

Equating coefficients at the same powers of ε, we arrive at the system of inhomogeneous differential equations with respect to corrections $\lambda_n^{(k)}(z)$ and $B_n^{(k)}(x,z)$:

$$L(n)B_n^{(0)}(x) = 0 \equiv f_n^{(0)}(z), \tag{28}$$

$$L(n)B_n^{(k)}(x,z) = (\lambda_n^{(k)}(z) - V^{(k)}(z))B_n^{(0)}(x) + \sum_{p=1}^{k-1}(\lambda^{(k-p)}(z) - V^{(k-p)}(z))B_n^{(p)}(x,z) \equiv f_n^{(k)}(z), \quad k \geq 1.$$

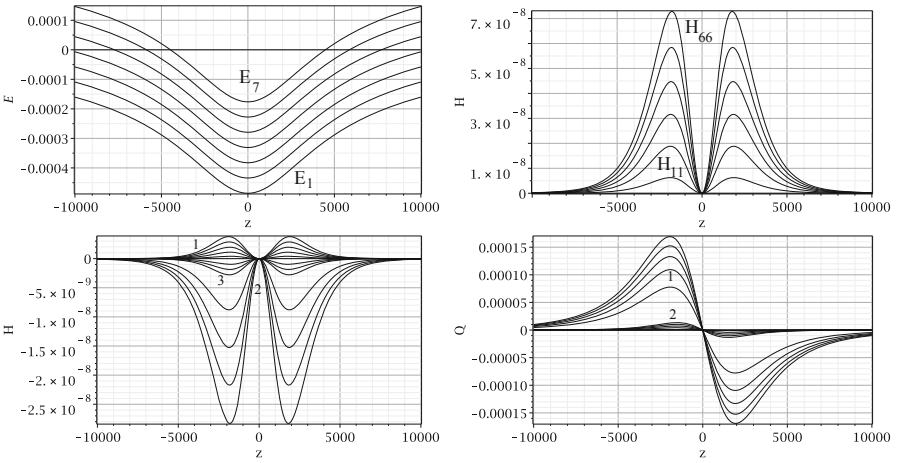

Fig. 3. The eigenvalues $E_j(z)$ and the effective potentials $H_{jj}(z)$, $H_{jj'}(z)$ (curves $H_{jj-1}(z)$, $j = 2, ..., 6$, are marked by number 1, curves $H_{jj-2}(z)$, $j = 3, ...6$, are marked by number 2 and curves $H_{jj-3}(z)$, $j = 4, ..., 6$, are marked by number 3) and $Q_{jj'}(z)$ (curves $Q_{jj-1}(z)$, $j = 2, ..., 6$, are marked by number 1, and curves $Q_{jj-2}(z)$, $j = 3, ..., 6$, are marked by number 2) for $m = -200$, $q = 1$, $\gamma = 2.553191 \cdot 10^{-5}$

To solve Eqs. (26) we used the *nonnormalized* orthogonal basis

$$B_{n+s}(x) = C_{n|m|} e^{-\frac{x}{2}} x^{\frac{|m|}{2}} L_{n+s}^{|m|}(x) = C_{n|m|} C_{n+s|m|}^{-1} B_{n+s,m}^{(0)}(x), \tag{29}$$
$$\langle s|s'\rangle = \int_0^\infty B_{n+s}(x) B_{n+s'}(x) dx = \delta_{ss'} \gamma \frac{n!}{(n+|m|)!} \frac{(n+s+|m|)!}{(n+s)!}.$$

The action of the operators $L(n)$ and x on the functions $B_{n+s}(x)$ is defined by the relations

$$L(n) B_{n+s}(x) = s B_{n+s}(x), \tag{30}$$
$$x B_{n+s}(x) = -(n+s+|m|) B_{n+s-1}(x) + (2(n+s)+|m|+1) B_{n+s}(x) - (n+s+1) B_{n+s+1}(x)$$

that involve no fractional powers of quantum numbers n and m.

Step 4. Applying Eqs. (30), the right-hand side $f_n^{(k)}(z)$ and the solutions $B_n^{(k)}(x, z)$ of the system (28) are expanded over the *nonnormalized* basis states $B_{n+s}(x)$

$$B_n^{(k)}(x, z) = \sum_{s=-s_{\max}}^{s_{\max}} b_{n;s}^{(k)}(z) B_{n+s}(x), \quad f_n^{(k)}(z) = \sum_{s=-s_{\max}}^{s_{\max}} f_{n;s}^{(k)}(z) B_{n+s}(x). \tag{31}$$

Then the recurrent set of linear algebraic equations for unknown *nonnormalized* coefficients $b_{n;s}^{(k)}(z)$ and corrections $\lambda_n^{(k)}(z)$ is obtained

$$s b_{n;s}^{(k)}(z) - f_{n;s}^{(k)}(z) = 0, \quad s = -s_{\max}, \ldots, s_{\max},$$

which is solved sequentially for $k = 1, 2, \ldots, k_{\max}$:

$$f_{n;0}^{(k)}(z) = 0 \quad \to \lambda_n^{(k)}(z); \quad b_{n;s}^{(k)}(z) = f_{n;s}^{(k)}(z)/s, \quad s = -s_{\max}, \ldots, s_{\max}, \quad s \neq 0.$$

The initial conditions (22) and $b_{n;s}^{(0)}(z) = \delta_{s0}$ follow from Eqs. (21) and (24).

Step 5. To obtain the normalized wave function $B_j(x; z)$ up to the kth order, the coefficient $b_0^{(k)}$ are defined by the following relation:

$$b_{n;0}^{(k)}(z) = -\frac{1}{2\gamma} \sum_{p=1}^{k-1} \sum_{s'=-s_{\max}}^{s_{\max}} \sum_{s=-s_{\max}}^{s_{\max}} b_{n;s}^{(k-p)}(z) \langle s|s'\rangle b_{n;s'}^{(p)}(z), \quad b_{n;0}^{(k=1)}(z) = 0.$$

As an example of the output file at steps 1–5, we display nonzero coefficients $\lambda_n^{(k)}(z)$, $b_{n;s}^{(k)}(z)$ of the expansions (27), (31) over the *nonnormalized* basis functions (29) up to $O(\varepsilon^2)$:

$$\begin{aligned}
&\lambda_n^{(0)} = n + (|m|+1)/2,\\
&\lambda_n^{(1)}(z) = -\frac{q}{\gamma\sqrt{z^2+2x_s}} + \frac{q(2n+|m|+1)}{\gamma^2(z^2+2x_s)^{3/2}} - \frac{x_s q}{\gamma(z^2+2x_s)^{3/2}},\\
&\lambda_n^{(2)}(z) = -q^2(2n+|m|+1)/(\gamma^4(z^2+2x_s)^3) - 3q[|m|^2+2+6n|m|\\
&\quad +6n^2+6n+3|m|-2\gamma(2n+|m|+1)x_s+x_s^2\gamma^2]/(2\gamma^3(z^2+2x_s)^{5/2}),\\
&b_{n;0}^{(0)}(z) = 1, \qquad (32)\\
&b_{n;-1}^{(1)}(z) = -q(n+|m|)/(\gamma^2(z^2+2x_s)^{3/2}), \quad b_{n;1}^{(1)}(z) = q(n+1)/(\gamma^2(z^2+2x_s)^{3/2}),\\
&b_{n;-2}^{(2)}(z) = q(n+|m|)(n+|m|-1)(2q-3\gamma\sqrt{(z^2+2x_s)})/(4\gamma^4(z^2+2x_s)^3),\\
&b_{n;-1}^{(2)}(z) = q(n+|m|)(2q+3\gamma(2n+|m|-\gamma x_s)\sqrt{(z^2+2x_s)})/(\gamma^4(z^2+2x_s)^3),\\
&b_{n;0}^{(2)}(z) = q^2(2n^2+2n+2n|m|+|m|+1)/(2\gamma^4(z^2+2x_s)^3),\\
&b_{n;1}^{(2)}(z) = -q(n+1)(2q+3\gamma(2n+|m|+2-\gamma x_s)\sqrt{(z^2+2x_s)})/(\gamma^4(z^2+2x_s)^3),\\
&b_{n;2}^{(2)}(z) = q(n+1)(n+2)(2q+3\gamma\sqrt{(z^2+2x_s)})/(4\gamma^4(z^2+2x_s)^3).
\end{aligned}$$

These expansions involve parameters $x_s = \rho_s^2/2$ and ρ_s that approximately corresponded to the minimum of the potential energy (2) and determined the point $x_0 = \gamma x_s$ of expansion of (25) of Coulomb potential $V_c(x, z)$.

Step 6. In terms of the scaled variable x, the expressions of the effective potentials $H_{ij}(z) = H_{ji}(z)$ and $Q_{ij}(z) = -Q_{ji}(z)$ take the form

$$H_{ij}(z) = \frac{1}{\gamma}\int_0^\infty dx \frac{\partial B_i(x;z)}{\partial z}\frac{\partial B_j(x;z)}{\partial z}, \quad Q_{ij}(z) = -\frac{1}{\gamma}\int_0^\infty dx B_i(x;z)\frac{\partial B_j(x;z)}{\partial z}. \quad (33)$$

To calculate them we expand the solution (26) over the *normalized* orthogonal basis $B_{n+s;m}^{(0)}(x)$ with the *normalized* coefficients $b_{n;n+s;m}^{(k)}(z)$,

$$B_j(x;z) \equiv B_j^m(x;z) = \sum_{k=0}^{k_{\max}} \varepsilon^k \sum_{s=-s_{\max}}^{s_{\max}} b_{n;n+s;m}^{(k)}(z) B_{n+s;m}^{(0)}(x). \qquad (34)$$

The normalized coefficients $b^{(k)}_{n;n+s;m}(z)$ are expressed via $b^{(k)}_{n;s}(z)$,

$$b^{(k)}_{n;n+s;m}(z) = b^{(k)}_{n;s}(z)\sqrt{\frac{n!}{(n+|m|)!}\frac{(n+s+|m|)!}{(n+s)!}} \tag{35}$$

as follows from Eqs. (31), (34), and (29).

Step 7. As a result of substituting Eqs. (34) into Eq. (33), the matrix elements take the form

$$\begin{aligned} Q_{jj+t}(z) &= -\sum_{k=0}^{k_{\max}} \varepsilon^k \sum_{k'=0}^{k} \sum_{s=\max(-s_{\max},-s_{\max}+t)}^{\min(s_{\max},s_{\max}+t)} b^{(k')}_{n;n+s;m}(z)\frac{db^{(k-k')}_{n+t;n+s;m}(z)}{dz}, \\ H_{jj+t}(z) &= \sum_{k=0}^{k_{\max}} \varepsilon^k \sum_{k'=0}^{k} \sum_{s=\max(-s_{\max},-s_{\max}+t)}^{\min(s_{\max},s_{\max}+t)} \frac{db^{(k')}_{n;n+s;m}(z)}{dz}\frac{db^{(k-k')}_{n+t;n+s;m}(z)}{dz}. \end{aligned} \tag{36}$$

By collecting the coefficients at similar powers of ε in Eq. (36) the algorithm yields the final expansions of eigenvalues and effective potentials available in the output file

$$E_j(z) = \sum_{k=0}^{k_{\max}} E^{(k)}_j(z),\ H_{ij}(z) = \sum_{k=2}^{k_{\max}} H^{(k)}_{ij}(z),\ Q_{ij}(z) = \sum_{k=1}^{k_{\max}} Q^{(k)}_{ij}(z). \tag{37}$$

Successful runs of the Maple implementation of the algorithm were performed up to $k_{\max} = 6$ (the run time 30 s using Intel Core i5, 3.36 GHz, 4 GB). Below we present a few first nonzero coefficients derived *in the analytic form* ($j = n + 1$):

$$E^{(0)}_j = 2\gamma(n + (m + |m| + 1)/2),$$

$$E^{(1)}_j(z) = -\frac{2q}{\sqrt{z^2+\rho_s^2}} + \frac{2q(2n+|m|+1)}{\gamma(z^2+\rho_s^2)^{3/2}} - \frac{\rho_s^2 q}{(z^2+\rho_s^2)^{3/2}},$$

$$E^{(2)}_j(z) = -\frac{2q^2(2n+|m|+1)}{\gamma^3(z^2+\rho_s^2)^3} - \frac{3q[|m|^2+2+6n|m|+6n^2+6n+3|m|-\gamma(2n+|m|+1)\rho_s^2+\rho_s^4\gamma^2/4]}{\gamma^2(z^2+\rho_s^2)^{5/2}},$$

$$Q^{(1)}_{jj-1}(z) = -\sqrt{n}\sqrt{n+|m|}\frac{3zq}{\gamma^2(z^2+\rho_s^2)^{5/2}},$$

$$Q^{(2)}_{jj-1}(z) = -\sqrt{n}\sqrt{n+|m|}\left[\frac{15zq(2|m|+4n-\rho_s^2\gamma)}{2\gamma^3(z^2+\rho_s^2)^{7/2}} + \frac{12zq^2}{\gamma^4(z^2+\rho_s^2)^4}\right],$$

$$Q^{(2)}_{jj-2}(z) = -\sqrt{n}\sqrt{n-1}\sqrt{n+|m|}\sqrt{n+|m|-1}\frac{15qz}{4\gamma^3(z^2+\rho_s^2)^{7/2}},$$

$$H^{(2)}_{jj}(z) = 9q^2(2n^2+2n|m|+2n+|m|+1)\left[\frac{1}{\gamma^4(z^2+\rho_s^2)^4} - \frac{\rho_s^2}{\gamma^4(z^2+\rho_s^2)^5}\right],$$

$$H^{(2)}_{jj-2}(z) = -9q^2\sqrt{n}\sqrt{n-1}\sqrt{n+|m|}\sqrt{n+|m|-1}\left[\frac{1}{\gamma^4(z^2+\rho_s^2)^4} + \frac{\rho_s^2}{\gamma^4(z^2+\rho_s^2)^5}\right].$$

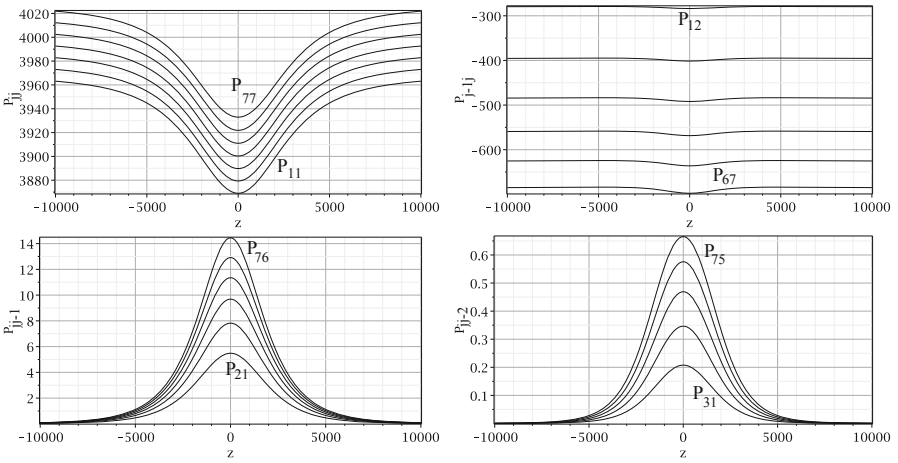

Fig. 4. Transverse dipole matrix elements $P_{nn'}^{|m||m|-1}$ (subscripts n, n' run $0, 1, 2, 3, 4, 5, 6$) for $m = -200$, $q = 1$, $\gamma = 2.553191 \cdot 10^{-5}$

As an example, Fig. 3 shows the eigenvalues and effective potentials (37), which agree with those calculated numerically using ODPEVP [10] with the accuracy of the order of 10^{-10}. We used finite element grid on the interval $\rho \in [\rho_{\min} = 2000, \rho_{\max} = 6000]$ with the Lagrange elements of fourth order. Expanding (37) into the Taylor series at $|z|/\rho_s \gg 1$, we arrive at perturbation expansion in powers of $1/z$ [8].

4 Calculations of the Transversal Dipole Matrix Elements

Using the scaled variable x defined by Eq. (18) one can express the transverse dipole matrix elements $P_{ij}^{|m|,|m|\mp1}(z) = \left\langle |m|, n \middle| \rho e^{\pm \imath\varphi} \middle| |m| \mp 1, n' \right\rangle$ and $P_{ij}^{-|m|,-|m|\pm1}(z) = \left\langle -|m|, n \middle| \rho e^{\mp \imath\varphi} \middle| -|m| \pm 1, n' \right\rangle$ possessing the property

$$\left\langle |m|, n \middle| \rho \exp(\pm \imath\varphi) \middle| |m| \mp 1, n' \right\rangle^* = \left\langle |m| \mp 1, n' \middle| \rho \exp(\mp \imath\varphi) \middle| |m|, n \right\rangle,$$

where $i = n + 1$ and $j = n' + 1$, in the following form

$$P_{ij}^{-|m|,-|m|\pm1}(z) = P_{ij}^{|m|,|m|\mp1}(z) = \sqrt{\frac{2}{\gamma^3}} \int_0^\infty dx B_i^{|m|}(x; z) \sqrt{x} B_j^{|m|\mp1}(x; z). \quad (38)$$

According to Eqs. (22.7.12), (33.7.30), and (22.7.31) of [14], the dipole moment matrix elements calculated with normalized basis functions $||m|, n\rangle = B_{n|m|}^{(0)}(x) e^{\imath|m|\varphi}/\sqrt{2\pi}$ by means of Eq. (23) are expressed as

$$P_{ij}^{(0);|m||m|\mp1} = \sqrt{\frac{2}{\gamma^3}} \left\langle |m|, n \middle| \sqrt{x} e^{\pm \imath\varphi} \middle| |m| \mp 1, n' \right\rangle$$

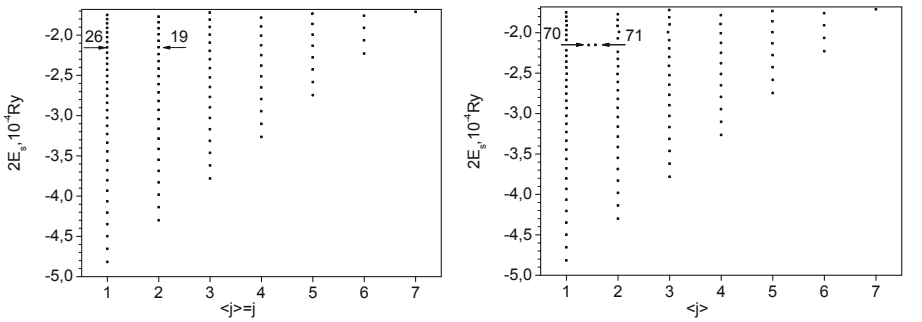

Fig. 5. Energy eigenvalues $2E_s$ for even ($\sigma = +1$) lower eigenstates vs the state number $\langle j \rangle$ calculated in the diagonal adiabatic approximation (left) and in the Kantorovich approximation at $j_{\max} = 6$ with given accuracy (right). Here $m = -200$, $\gamma = 2.553191 \cdot 10^{-5}$, $q = 1$, $\sigma = +1$. The quantity $\langle j \rangle = \sum_j \int j \chi_{j,s}(z)^2 dz$ is the averaged quantum number, s is the eigenvalue number in the ascending energy sequence $E_1 < E_2 < ... < E_s < ... < \gamma/2$, corresponding to the number v of the eigenvalue $E_{j1} < E_{j2} < ... < E_{jv} < ... < \gamma/2$ counted at each $\langle j \rangle = j$ in diagonal approximation (17) of Eqs. (12)

$$= \sqrt{\frac{2}{\gamma^3}} \frac{1}{2\pi} \int_0^{2\pi} d\varphi \int_0^{\infty} e^{-\imath |m| \varphi} B^{(0)}_{i,|m|}(x) e^{\pm \imath \varphi} \sqrt{x} e^{\imath (|m| \mp 1)\varphi} B^{(0)}_{i,|m|\mp 1}(x) dx$$
$$= \sqrt{\frac{2}{\gamma}} \Big[\delta_{nn'} \sqrt{n + |m| + 1/2 \mp 1/2} - \delta_{n\mp 1,n'} \sqrt{n + 1/2 \mp 1/2} \Big]. \quad (39)$$

As a result of substituting Eqs. (34) and (39) into Eq. (38), the matrix elements take the following *analytic* form ($j = n + 1$)

$$P^{|m|,|m|-1}_{jj+t}(z) = \sum_{k=0}^{k_{\max}} P^{(k);|m||m|-1}_{jj+t}(z),$$
$$P^{(k);|m||m|-1}_{jj+t}(z) = \sqrt{\frac{2}{\gamma}} \sum_{k'=0}^{k} \sum_{s=\max(-k,k'-k-t)}^{\min(k,k-k'-t)} \Big[b^{(k')}_{n;n+s;|m|}(z) b^{(k-k')}_{n+t;n+s;|m|-1}(z)$$
$$\times \sqrt{n + s + |m| + 1} - b^{(k')}_{n;n+s;|m|}(z) b^{(k-k')}_{n+t;n+s+1;|m|-1}(z) \sqrt{n + s + 1} \Big]. \quad (40)$$

Successful run of the Maple-implemented algorithm was performed up to $k_{\max} = 6$ (run time 90 s with Intel Core i5, 3.36 GHz, 4 GB). A few first nonzero coefficients derived *in the analytic form* are presented below ($j = n + 1$):

$$P^{(0);|m||m|-1}_{jj}(z) = +\frac{\sqrt{2}\sqrt{n + |m| + 1}}{\sqrt{\gamma}}, P^{(1);|m||m|-1}_{jj}(z) = -\frac{\sqrt{2}\sqrt{n + |m|} q}{\gamma^{5/2}(\rho_s^2 + z^2)^{3/2}},$$
$$P^{(0);|m||m|-1}_{j-1j}(z) = -\frac{\sqrt{n}\sqrt{2}}{\sqrt{\gamma}}, \quad (41)$$
$$P^{(1);|m||m|-1}_{j-1j}(z) = -\frac{\sqrt{n}\sqrt{2}\sqrt{n + |m|}(\sqrt{n + |m| - 1} - \sqrt{n + |m| + 1}) q}{(\rho_s^2 + z^2)^{3/2}\gamma^{5/2}},$$

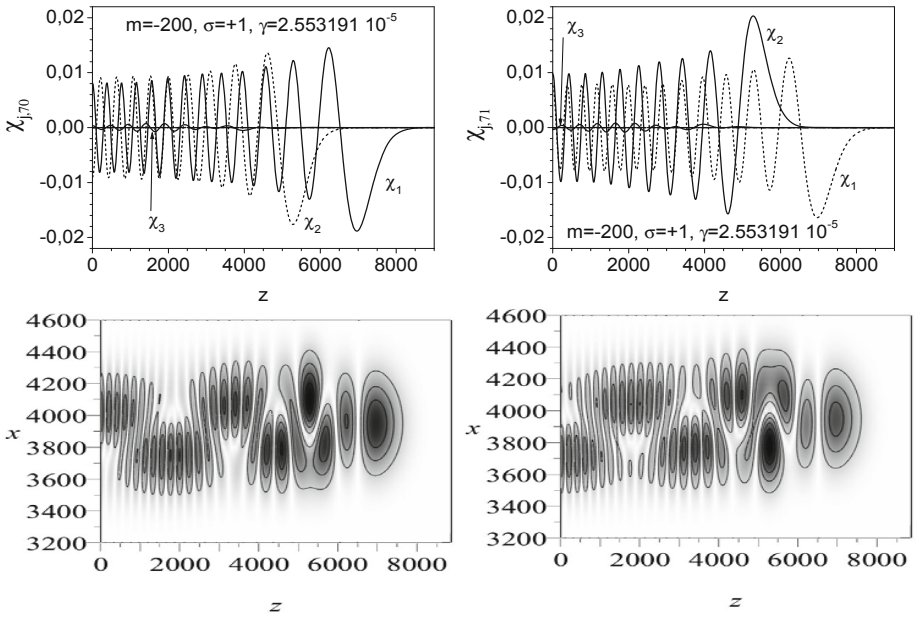

Fig. 6. Upper panels: the first three components of the eigenfunctions $\chi_{j,70}$ and $\chi_{j,71}$ ($j = 1, 2, 3$). The dominant components are $j = 1$ ($\langle j \rangle = 1.43$) with $v - 1 = 25$ nodes and $j = 2$ ($\langle j \rangle = 1.56$) with $v - 1 = 18$ nodes, respectively. Lower panels: the profile of the wave function $\Psi_{s=70}^{m=-200,\sigma=+1}(\rho, z)$ and $\Psi_{s=71}^{m=-200,\sigma=+1}(\rho, z)$ of the *resonance states* in the zx plane with the energies $2E_{s=70}^{m=-200,\sigma=+1} = -2.151832 \cdot 10^{-4}$Ry and $2E_{s=71}^{m=-200,\sigma=+1} = -2.150977 \cdot 10^{-4}$Ry pointed by arrows in the right panel of Fig. 5

$$P_{jj-1}^{(1);|m||m|-1}(z) = \frac{\sqrt{n}\sqrt{2}(\sqrt{n+|m|-1}\sqrt{n+|m|+1} - n - |m|)q}{(\rho_s^2 + z^2)^{3/2}\gamma^{5/2}}.$$

The comparison of our analytical numerical results with those obtained numerically using the program ODPEVP [10] shows the convergence of the perturbation series expansion up to $k_{\max} = 6$ with four significant digits. Expanding (40) into a Taylor series at $|z|/\rho_s \gg 1$, we arrive at the inverse power series for the dipole matrix elements. To obtain the leading terms at $|z| \to \infty$ it is sufficiently to put $\rho_s = 0$ in (41).

5 Calculations of Rydberg States and Decay Rates

In Fig. 5 we present an example of the lower part of discrete spectrum calculated in the diagonal adiabatic and Kantorovich approximations with the effective potentials (37) by means of the program KANTBP2 [1]. In numerical calculations at $q = -1$, $\gamma = 2.553191 \cdot 10^{-5}$ for $|m| \sim 200$, we use finite element grid on the interval $z \in [0, z_{\max} = 11000]$ with the Lagrange elements of fourth order. In

Fig. 6, we show an example of resonance states formed by coupling of the quasi-degenerate states with the energies $2E_{j=1,v=26}^{m=-200,\sigma=+1} = -2.151260 \cdot 10^{-4}$Ry and $2E_{j=2,v=19}^{m=-200,\sigma=+1} = -2.151202 \cdot 10^{-4}$Ry in the diagonal adiabatic approximation (17) pointed by arrows in the left panel of Fig. 5.

The partial transition decay rates $\Gamma_{\tilde{s}\to\tilde{s}'}$ are calculated as

$$\Gamma_{\tilde{s}\to\tilde{s}'} = \frac{4}{3}\frac{e^2\omega_{\tilde{s}\tilde{s}'}^3}{4\pi\varepsilon_0\hbar c^3}|\langle\tilde{s}'|\bar{\mathbf{r}}|\tilde{s}\rangle|^2, \quad \omega_{\tilde{s}\tilde{s}'} = (\bar{E}_{\tilde{s}'} - \bar{E}_{\tilde{s}})/\hbar. \tag{42}$$

In the above expressions, $\varepsilon_0 = 8.854187817 \cdot 10^{-12}$ F/m is the dielectric constant, the energy $\bar{E}_{\tilde{s}'} = E_{\tilde{s}'}E_B$ and the dipole moment $\langle\tilde{s}'|\bar{\mathbf{r}}|\tilde{s}\rangle = a_B\langle\tilde{s}'|\mathbf{r}|\tilde{s}\rangle$ are expressed in the atomic units $E_B = 2Ry = 4.35974434 \cdot 10^{-18}$ J, $a_B = 0.52917721092 \cdot 10^{-10}$ m, i.e.

$$\Gamma_{\tilde{s}\to\tilde{s}'} = 2.142 \cdot 10^{10}(E_{\tilde{s}'} - E_{\tilde{s}})^3|\langle\tilde{s}'|\mathbf{r}|\tilde{s}\rangle|^2 \times \mathrm{s}^{-1}. \tag{43}$$

Here $|\langle\tilde{s}'|\mathbf{r}|\tilde{s}\rangle|^2$ defined by the expression

$$|\langle\tilde{s}'|\mathbf{r}|\tilde{s}\rangle|^2 = (1/2)|\langle\tilde{s}'|\rho e^{-\imath\varphi}|\tilde{s}\rangle|^2 + |\langle\tilde{s}'|z|\tilde{s}\rangle|^2 + (1/2)|\langle\tilde{s}'|\rho e^{+\imath\varphi}|\tilde{s}\rangle|^2, \tag{44}$$

where $\langle\tilde{s}'|z|\tilde{s}\rangle$ and $\langle\tilde{s}'|\rho e^{\pm\imath\varphi}|\tilde{s}\rangle$ are the longitudinal and transverse dipole moment, respectively. As follows from Eq. (40),

$$\langle\tilde{s}'|z|\tilde{s}\rangle = \delta_{m'm}\delta_{-\sigma'\sigma}\sum_{i,j=1}^{j_{\max}}\int_{z_{\min}}^{z_{\max}} dz\chi_{i\tilde{s}'}^{m\sigma'}(z)z\chi_{j\tilde{s}}^{m\sigma}(z), \tag{45}$$

$$\langle\tilde{s}'|\rho e^{\pm\imath\varphi}|\tilde{s}\rangle = \delta_{m'm\mp1}\delta_{\sigma'\sigma}\sum_{i,j=1}^{j_{\max}}\int_{z_{\min}}^{z_{\max}} dz\chi_{i\tilde{s}'}^{m'\sigma}(z)P_{ij}^{m',m}(z)\chi_{j\tilde{s}}^{m\sigma}(z). \tag{46}$$

In Table 1 we show our present results for partial decay rates (43) and dipole moments (45) and (46). The results were obtained numerically by means of the program KANTBP 2.0 [1] using the analytically derived effective potentials (37) and matrix elements of transversal dipole moments (40), i.e., $M_{\tilde{s}'\tilde{s}} = \langle\tilde{s}'|\rho e^{-\imath\varphi}|\tilde{s}\rangle$ for cyclotron decay (C) ($q \to q' = q$, where $q = j - m$ is magnetron quantum number, $m \to m' = m - 1$, $\sigma \to \sigma' = \sigma$, $j \to j' = j - 1$, $v \to v' = v$); $M_{\tilde{s}'\tilde{s}} = \langle\tilde{s}'|z|\tilde{s}\rangle$ for the bounce decay (B) ($q \to q' = q$, $m \to m' = m$, $\sigma \to \sigma' = -\sigma$, $j \to j' = j$, $v \to v' = v - 1$), and $M_{\tilde{s}'\tilde{s}} = \langle\tilde{s}'|\rho e^{+\imath\varphi}|\tilde{s}\rangle$ for the magnetron decay (M) ($q \to q' = q - 1$, $m \to m' = m + 1$, $\sigma \to \sigma' = \sigma$, $j \to j' = j$, $v \to v' = v$). The results agree with the numerical ones from [12] within the required accuracy.

In Table 1 we also show the energy values $2E_{|\tilde{s}\rangle}$ calculated in the Kantorovich approximation (K) at $j_{\max} = 6$, and obtained by the aid of the diagonal approximation (17) in the *analytical form*

$$2E_{|\tilde{s}\rangle} \approx 2E_{i,v}^{m,\sigma} = U_{ii}^{(0)} + \mathcal{E}_{i;v}^{(0)} + \sum\nolimits_{\kappa=2}^{\kappa_{\max}}\mathcal{E}_{i;v}^{(\kappa-1)}, \tag{47}$$

$$\mathcal{E}_{i;v}^{(0)} = \omega_{z,i}(2v+1), \quad \mathcal{E}_{i;v}^{(1)} = \frac{3U_i^{(4)}(2v^2+2v+1)}{4\omega_{z,i}^2},$$

$$\mathcal{E}_{i;v}^{(2)} = -\frac{(2v+1)(17v^2+17v+21)(U_i^{(4)})^2}{16\omega_{z,i}^5} + \frac{5(2v+1)(2v^2+2v+3)U_i^{(6)}}{8\omega_{z,i}^3}.$$

Table 1. The partial transition decay rates $\Gamma_{\tilde{s}\to\tilde{s}'}$ evaluated using Eq. (43) from the state $|\tilde{s}\rangle = |j,v,\sigma,m\rangle$ to $|\tilde{s}'\rangle = |j',v',\sigma',m'\rangle$ with energies $2E_{|\tilde{s}\rangle}$ and $2E_{|\tilde{s}'\rangle}$ calculated using the Kantorovich approximation (K) at $j_{\max} = 6$ and the corresponding dipole moments $M_{\tilde{s}'\tilde{s}}$. In square brackets, numerical results of [12] are given. The energies calculated in *analytical form* using the crude diagonal approximation with the Taylor series of $U_{ii}(z) = E_i(z)$ up to harmonic (H) and anharmonic (A) terms of order of z^2 and z^{10}, respectively. The corresponding energies in the diagonal approximation with Taylor series of $U_{ii}(z) = E_i(z) + H_{ii}(z)$ differing only in two last digits, are shown in parentheses.

	$\tilde{s}$	$\tilde{s}'$	$\lvert j,v,\sigma,m\rangle$	$\lvert j',v',\sigma',m'\rangle$	$\Gamma_{\tilde{s}\to\tilde{s}'}$, s^{-1}	$M_{\tilde{s}'\tilde{s}}$, a_B		$2E_{\tilde{s}}$, 10^{-4}Ry	$2E_{\tilde{s}'}$, 10^{-4}Ry
C	5	1	$\lvert 2,1,+1,-200\rangle$	$\lvert 1,1,+1,-201\rangle$	13.1	276.4	K	−4.29933	−4.80384
					[13.7]	[283]	H	−4.29978(76)	−4.80384(83)
							A	−4.30019(18)	−4.80424(23)
C	13	5	$\lvert 3,1,+1,-200\rangle$	$\lvert 2,1,+1,-201\rangle$	26.3	390.9	K	−3.78171	−4.28632
					[27.5]	[401]	H	−3.78299(95)	−4.28688(86)
							A	−3.78342(38)	−4.28729(27)
B	1	1	$\lvert 1,2,-1,-200\rangle$	$\lvert 1,1,+1,-200\rangle$	0.180	349.4	K	−4.73499	−4.81688
					[0.178]	[350]	H	−4.73329(27)	−4.81683(83)
							A	−4.73531(29)	−4.81724(23)
B	2	1	$\lvert 1,3,+1,-200\rangle$	$\lvert 1,2,-1,-200\rangle$	0.345	499.0	K	−4.65469	−4.73499
					[0.342]	[500]	H	−4.64974(71)	−4.73329(27)
							A	−4.65497(94)	−4.73531(29)
M	1	1	$\lvert 1,1,+1,-200\rangle$	$\lvert 1,1,+1,-199\rangle$	0.045	3870	K	−4.81688	−4.83003
					[0.044]	[3872]	H	−4.81683(83)	−4.82993(93)
							A	−4.81724(23)	−4.83034(33)

The latter was obtained using SNA like in Section 3, but for a perturbed 1D oscillator with *adiabatic frequency* $\omega_{z,i}$. It was accomplished with the help of a Taylor expansion up to $z^{2\kappa_{\max}}$ of effective potentials $U_{ii}(z) = E_i(z) + H_{ii}(z)$ from Eq. (37) for the harmonic (H) and anharmonic (A) terms, i.e., $2\kappa_{\max} = 2$ and $2\kappa_{\max} = 10$, respectively,

$$U_{ii}(z) = U_{ii}(0) + \omega_{z,i}^2 z^2 + \sum\nolimits_{\kappa=2}^{\kappa_{\max}} U_i^{(2\kappa)} z^{2\kappa}. \tag{48}$$

Moreover, in Table 1 we present also the results for the energies (47) in the crude and adiabatic approximations obtained without and with the diagonal potential H_{ii}, respectively. One can see that the energies in crude adiabatic and adiabatic approximations differ only in two last significant figures, i.e., are the same within the accuracy of $\sim 10^{-8}$. One can see from Table 1 that the adiabatic harmonic (H) diagonal approximation and the crude anharmonic (A) one provide the *upper and lower estimations of the energy values of low-excited Rydberg states* with $j = 1$, respectively.

Remark 2. In the expansions (47) and (48), the coefficients are calculated using $U_{ii}^{(0)} = U_{ii}(0)$, $\omega_{z,i}^2 = (d^2U_{ii}(z)/dz^2)_{z=0}/2$, $U_i^{(2\kappa)} = (d^{2\kappa}U_{ii}(z)/dz^{2\kappa})_{z=0}/((2\kappa)!)$.

In the harmonic approximation $\omega_{z,i}^2 = \sum_{k=1}^{k_{\max}} \omega_{z,i,E}^{(k)} + \sum_{k=2}^{k_{\max}} \omega_{z,i,H}^{(k)}$, where $\omega_{z,i,E}^{(k)} = (d^2 E_i^{(k)}(z)/dz^2)_{z=0}/2$ and $\omega_{z,i,H}^{(k)} = (d^2 H_{ii}^{(k)}(z)/dz^2)_{z=0}/2$, the leading terms are:

$$\omega_{z,i,E}^{(1)} = \frac{5q}{2\rho_s^3} - \frac{3q(2n+|m|+1)}{\gamma\rho_s^5}, \quad \omega_{z,i,H}^{(2)} = \frac{9q^2(2n^2+2n|m|+2n+|m|+1)}{\rho_s^{10}\gamma^4},$$

$$\omega_{z,i,E}^{(2)} = \frac{15q}{8\rho_s^3} - \frac{15q(2n+|m|+1)}{2\gamma\rho_s^5} + \frac{15q(6n^2+6n|m|+6n+m^2+3|m|+2)}{2\gamma^2\rho_s^7} + \frac{6q^2(2n+|m|+1)}{\gamma^3\rho_s^8}.$$

The substitution of $\rho_s = \sqrt{2|m|/\gamma}$ into the leading term $\omega_{z,i}^2 \approx \omega_{z,i,E}^{(1)}$ at $n = 0$ yields $\omega_{z,i}^2 \approx (q\sqrt{\gamma}\gamma(2|m|-3))/(4m^2\sqrt{2|m|})$. At $q = 1$ we obtain the *adiabatic parameter* $(\omega_\rho/\omega_{z,i=1})^{4/3} = |m|\gamma^{1/3}$, where $\omega_\rho = \gamma/2$, in agreement with [13].

6 Conclusions

A new efficient method to calculate wave functions and decay rates of high-$|m|$ Rydberg states of a hydrogen atom in a magnetic field is developed. It is based on the KM application to parametric eigenvalue problems in cylindrical coordinates. The results are in a good agreement with the calculations executed in spherical coordinates at fixed $|m| > 140$ for $\gamma \sim 2.553 \cdot 10^{-5}$. The elaborated SNA for calculation of the effective potentials, dipole moment matrix elements, and the perturbation solutions *in analytic form* allows us to generate effective approximations for a finite set of longitudinal equations. This provides benchmark calculations for the new version KANTBP3 of our earlier program KANTBP2 [1] announced in [9]. The developed approach is a useful tool for calculating the threshold phenomena in formation, decay, and ionization of (anti)hydrogen-like atoms and ions in magneto-optical traps [11,12,13], and channelling of ions in thin films [4].

The authors thank Prof. V.L. Derbov for valuable discussions.

References

1. Chuluunbaatar, O., Gusev, A.A., Vinitsky, S.I., Abrashkevich, A.G.: KANTBP 2.0: New version of a program for computing energy levels, reaction matrix and radial wave functions in the coupled-channel hyperspherical adiabatic approach. Phys. Commun. 179, 685–693 (2008)
2. Gusev, A., Gerdt, V., Kaschiev, M., Rostovtsev, V., Samoylov, V., Tupikova, T., Vinitsky, S.: A Symbolic-Numerical Algorithm for Solving the Eigenvalue Problem for a Hydrogen Atom in Magnetic Field. In: Ganzha, V.G., Mayr, E.W., Vorozhtsov, E.V. (eds.) CASC 2006. LNCS, vol. 4194, pp. 205–218. Springer, Heidelberg (2006)
3. Chuluunbaatar, O., Gusev, A.A., Derbov, V.L., Kaschiev, M.S., Melnikov, L.A., Serov, V.V., Vinitsky, S.I.: Calculation of a hydrogen atom photoionization in a strong magnetic field by using the angular oblate spheroidal functions. J. Phys. A 40, 11485–11524 (2007)

4. Gusev, A.A., Derbov, V.L., Krassovitskiy, P.M., Vinitsky, S.I.: Channeling problem for charged particles produced by confining environment. Phys. At. Nucl. 72, 768–778 (2009)
5. Chuluunbaatar, O., Gusev, A.A., Gerdt, V.P., Rostovtsev, V.A., Vinitsky, S.I., Abrashkevich, A.G., Kaschiev, M.S., Serov, V.V.: POTHMF: A program for computing potential curves and matrix elements of the coupled adiabatic radial equations for a hydrogen-like atom in a homogeneous magnetic field. Comput. Phys. Commun. 178, 301–330 (2008)
6. Gusev, A.A., Chuluunbaatar, O., Gerdt, V.P., Rostovtsev, V.A., Vinitsky, S.I., Derbov, V.L., Serov, V.V.: Symbolic-Numeric Algorithms for Computer Analysis of Spheroidal Quantum Dot Models. In: Gerdt, V.P., Koepf, W., Mayr, E.W., Vorozhtsov, E.V. (eds.) CASC 2010. LNCS, vol. 6244, pp. 106–122. Springer, Heidelberg (2010); arXiv:1104.2292
7. Vinitsky, S.I., Chuluunbaatar, O., Gerdt, V.P., Gusev, A.A., Rostovtsev, V.A.: Symbolic-Numerical Algorithms for Solving Parabolic Quantum Well Problem with Hydrogen-Like Impurity. In: Gerdt, V.P., Mayr, E.W., Vorozhtsov, E.V. (eds.) CASC 2009. LNCS, vol. 5743, pp. 334–349. Springer, Heidelberg (2009)
8. Chuluunbaatar, O., Gusev, A., Gerdt, V., Kaschiev, M., Rostovtsev, V., Samoylov, V., Tupikova, T., Vinitsky, S.: A Symbolic-Numerical Algorithm for Solving the Eigenvalue Problem for a Hydrogen Atom in the Magnetic Field: Cylindrical Coordinates. In: Ganzha, V.G., Mayr, E.W., Vorozhtsov, E.V. (eds.) CASC 2007. LNCS, vol. 4770, pp. 118–133. Springer, Heidelberg (2007)
9. Gusev, A.A., Vinitsky, S.I., Chuluunbaatar, O., Gerdt, V.P., Rostovtsev, V.A.: Symbolic-Numerical Algorithms to Solve the Quantum Tunneling Problem for a Coupled Pair of Ions. In: Gerdt, V.P., Koepf, W., Mayr, E.W., Vorozhtsov, E.V. (eds.) CASC 2011. LNCS, vol. 6885, pp. 175–191. Springer, Heidelberg (2011)
10. Chuluunbaatar, O., Gusev, A.A., Vinitsky, S.I., Abrashkevich, A.G.: ODPEVP: A program for computing eigenvalues and eigenfunctions and their first derivatives with respect to the parameter of the parametric self-adjoined Sturm-Liouville problem. Comput. Phys. Commun. 180, 1358–1375 (2009)
11. Chuluunbaatar, O., Gusev, A.A., Vinitsky, S.I., Derbov, V.L., Melnikov, L.A., Serov, V.V.: Photoionization and recombination of a hydrogen atom in a magnetic field. Phys. Rev. A 77, 034702–1–034702–4 (2008)
12. Guest, J.R., Choi, J.-H., Raithel, G.: Decay rates of high-|m| Rydberg states in strong magnetic fields. Phys. Rev. A 68, 022509–1–022509–9 (2003)
13. Guest, J.R., Raithel, G.: High-|m| Rydberg states in strong magnetic fields. Phys. Rev. A 68, 052502–1–052502–9 (2003)
14. Abramovits, M., Stegun, I.A.: Handbook of Mathematical Functions. Dover, New York (1972)